



HAL
open science

New advances in triboelectrochemistry: from steady state to impedance of abraded stainless steel in acidic medium

Michel Keddam, Feng Liao, Pierre Ponthiaux, Vincent Vivier

► **To cite this version:**

Michel Keddam, Feng Liao, Pierre Ponthiaux, Vincent Vivier. New advances in triboelectrochemistry: from steady state to impedance of abraded stainless steel in acidic medium. *Journal of Solid State Electrochemistry*, 2015, 19, pp.2591-2599. 10.1007/s10008-015-2914-8 . hal-01197093

HAL Id: hal-01197093

<https://hal.sorbonne-universite.fr/hal-01197093>

Submitted on 11 Sep 2015

HAL is a multi-disciplinary open access archive for the deposit and dissemination of scientific research documents, whether they are published or not. The documents may come from teaching and research institutions in France or abroad, or from public or private research centers.

L'archive ouverte pluridisciplinaire **HAL**, est destinée au dépôt et à la diffusion de documents scientifiques de niveau recherche, publiés ou non, émanant des établissements d'enseignement et de recherche français ou étrangers, des laboratoires publics ou privés.

New advances in triboelectrochemistry: From steady-state to impedance of abraded stainless steel in acidic medium

Michel Keddam,^{1,*} Feng Liao,² Pierre Ponthiaux,^{2,*} Vincent Vivier^{1,*}

1. Sorbonne Universités, UPMC Univ Paris 06, UMR 8235, Laboratoire Interfaces et Systèmes Electrochimiques, F-75005, Paris, France

2. Laboratoire LGPM, Ecole Centrale, Rue des Vignes, 92290 Châtenay-Malabry, 5 France

Abstract

The present paper reports on the application of EIS in triboelectrochemistry. Electrochemical measurements were performed at the constant dc current attained during a permanent regime of friction achieved by a rotating Pin-on-Disc (P-o-D) tribometer. A model is then proposed which embodies a classical kinetic description of an active-passive transition into the accepted description of the tribo-electrochemical response of a passive material. From the derivation of the equation at steady-state, a set of parameters were determined allowing to describe correctly both the dc and ac behaviours of the interface and to estimate the different components of the tribo-electrochemical signals.

Keywords: *electrochemical impedance spectroscopy, repassivation, dissolution, tribocorrosion, electrochemical modeling.*

*Corresponding authors: michel.keddam@upmc.fr
pierre.ponthiaux@ecp.fr
vincent.vivier@upmc.fr

1. Introduction

Triboelectrochemistry or tribocorrosion studies by electrochemical techniques are based on the measurement of the current flowing from an abraded metal surface under both well-defined mechanical and electrochemical conditions (medium composition and polarization). The interpretation of the data most generally relies on a model of interaction of the abrading body with the surface of the material, which generates a bare interface (so-called fresh surface) by removing both the protective layer and some underlying material. The electrochemical response is ascribed to the recovery of the surface conditions by several simultaneous processes including build-up of the double layer, growth of a new surface film, dissolution of the transitory unprotected metal... The main goal is to better understand the reciprocal or synergetic interaction between mechanical and reactive contributions to the overall tribocorrosion process. Most of the works in the field have remained restricted to steady state (current to voltage curves) [1-6] or transient techniques [5,7,8] aimed at separating the individual contributions of the film growth and that of the metal dissolution to the total wear. Most powerful techniques in the field of electrochemical corrosion mechanism and particularly complex electrochemical impedance spectroscopy in a wide frequency range, EIS, have been very scarcely used [5]; but no electrochemical model addressing the ac response of a transient current being available, they remained at a strictly descriptive level.

Basically, the electrochemical response depends on 3 parameters: the load, the sliding velocity of the abrading body and the electrochemical polarisation, either potentiostatic or galvanostatic, of the sample. An impedance approach can be performed by modulating any of these three parameters allowing transfer functions to be studied. For instance, it was shown recently [8] that a Tribo-Electrochemical-Impedance, TEI, defined from the superposition of an *ac* component on the sliding velocity, gives access to the shape of the transient current density response. The present paper is dealing with the application of EIS in

triboelectrochemistry. Measurements were performed at the constant dc current attained during a permanent regime of friction achieved by a rotating Pin-on-Disc (P-o-D) tribometer. A model is proposed which embodies a classical kinetic description of an active-passive transition into the accepted description of the tribo-electrochemical response of a passive material [9]. The set of parameters allows to describe correctly both the dc and ac behaviours of the interface and to estimate the different components of the tribo-electrochemical signals.

2. Theoretical background

2.1. General properties of the formal dc and ac responses.

After the first rotations, a permanent regime of friction is reached by the P-o-D tribometer, and the surface relaxation behind the plot is supposed to generate a current density vs time transient, $j(\sigma)$, where σ is the time variable referring to the position of the sliding abrasive body (at $\sigma = 0$). To fulfil a finite charge condition, $j(t)$ must be integrable. The total current flowing to the abraded area of length L is given by the sum of the local current density along the wear:

$$I(L) = w \int_0^L j\left(\frac{x}{v}\right) dx \quad (1)$$

Where v is the constant velocity of the abrading body, x the position variable, and w the width of the abraded track. It should be mentioned that the more general case of a time dependent velocity has been dealt with in [8].

By changing the variable from x to σ :

$$I(T) = w \int_0^{\frac{L}{v}} v j(\sigma) d\sigma = w v \int_0^T j(\sigma) d\sigma \quad (2)$$

where T is the time-window considered in the experiment. In the case of a P-o-D tribometer it corresponds to the rotation period of the device.

The easiest description of the variation of $j(\sigma)$ is to use an exponential decay, such as:

$$j(\sigma) = j_0 \exp\left(\frac{-\sigma}{\tau}\right) \quad (3)$$

where τ is the time-constant. This description is considered in this paper for two main reasons:

- it is a decreasing, integrable and easy to handle function;
- it is often involved in the formal modelling of physical systems being controlled by first order linear differential equations. This is the case in many descriptions of electrochemical interfaces by heterogeneous reactions coupled by surface intermediates, like dissolution and film growth. It must be pointed out that the treatment below is not strictly limited to an exponential response. It remains valid for any decreasing, integrable function tending towards 0 at reasonable σ values.

From Eq. 3, the constant current generated by a P-o-D with a rotation period T is given by:

$$I(T) = w v j_0 \tau \left[1 - \exp\left(\frac{-T}{\tau}\right) \right] \quad (4)$$

The electrochemical processes taking place in the transient range are sketched in Fig.1. The double layer charging, generally considered as of much smaller order of magnitude [4] is neglected.

Compared to classical interfacial electrochemistry, the situation generated by this experiment is totally exotic: at a given fixed distance, whether in space or time scale, behind the abrading

body the electrochemical state of the interface is time-independent even though in an unsteady-state on the whole track. The response can thus be depicted as a “travelling transient” of which each point is in the same electrochemical state regardless of the pin position on the track. As a result, the system behaves as a steady-state one allowing EIS to be performed and modelled. The overall current density given by Eqs. 2 and 4 is a space or time averaged quantity. These two components cannot be separated by measuring only the dc current I , nor by analysing the ac response to a modulation of the rotation rate [8]. The present paper is essentially aimed at proposing a general way for modelling the ac response of the overall current, illustrating this procedure by a simple electrochemical model and applying it to the behaviour of stainless steel passivated in an acidic solution. In some extent the same goals were addressed in [10] but based on potentiostatic transients subjected to more questionable assumptions.

The same procedure previously developed for the dc current can be applied for deriving the impedance of the whole track by summing the local ac current densities induced by a sine wave modulation of the applied potential, as shown in Fig. 2.

From Eq. 2, the ac potential modulation $|\Delta E|\exp(j\omega t)$ being applied at every point of the transient, the ac component of the overall current flowing between 0 and T is given by:

$$\Delta I(T, j\omega) = w \cdot v \cdot |\Delta E| \exp(j\omega t) \int_0^T a(E_0, \sigma, j\omega) \cdot d\sigma \quad (5)$$

The local admittance density $a(E_0, \sigma, j\omega)$ is fixed by the local electrochemical state of the interface at the position σ or $x = v\sigma$. In the next section, its expression will be derived in the framework of a dissolution-repassivation model.

Therefore, like for a traditional electrode, the electrochemical behaviour of the electrode under abrasion is made available through both its dc current and its impedance spectrum. It

must be emphasised that the local current densities profiles (both dc and ac components) could be determined directly by using a micro current probe like a scanning vibrating electrode technique (SVET) [11-13] or a bi-microreference electrode [14,15] attached to the pin, a device not already implemented.

2.2. Mechanistic model

The sketch of the kinetic model shown in Fig. 3 is well-known and generally adopted for interpreting the anodic behaviour of pure metals and alloys in media covering a broad range of aggressiveness. Steady-state current-voltage curves as well as impedance and rotating ring-disc electrode (RRDE) behaviour in a wide frequency domain, displaying inductances and/or negative resistance are explained by the relaxation of one (or several) surface coverage under control by the mass balance between coupled reaction steps [16-18].

This basic model consists of:

- a single-step for the dissolution of the bare metal, that takes place on the surface fraction $(1-\theta)$. Only one metallic species is considered in this work (which can correspond to a pure metal). A slight solubility of the passive film can be added to the model, with no influence in the case dealt in this paper.
- a reversible single step describing film-forming reaction on the surface fraction θ . The coverage θ is assumed to obey a Langmuir isotherm.

The derivation of the steady-state and ac behaviours are essentially based on the mass and charge balances resulting from the reactions. The coverage θ is controlled by the balance between the film forming step of rate, $K_p(1-\theta)$, and the film dissolution of rate, $K'_p \theta$, expressed by Eq. 6.

$$\frac{\beta d\theta}{dt} = K_p(1-\theta) - K'_p \theta \quad (6)$$

where β is the surface concentration of the film material in moles.cm⁻².

In this case, experiments were performed at a constant dc-potential and due to the use of a Langmuir isotherm, Eq. 6 results in a linear differential equation with first order constant coefficients giving rise to a straightforward analytical solution. In the general case, such as time dependent K values, higher order reaction rates, or non-Langmuir isotherm, this equation must be solved numerically.

The current density through the interface is, at any time, given by the Faraday equivalent of the reaction rate for the instant values of the potential and of the surface coverage θ . It contains two parallel components due to the healing of the damage by film regrowth, j_p , and the dissolution of the incompletely protected metal, j_d .

$$j = \frac{I}{S} = F \left[z_p (K_p (1-\theta) - K'_p \theta) + z_d K_d (1-\theta) \right] \quad (7)$$

where z_p and z_d are the numbers of electrons exchanged in the corresponding reactions, S the interface area and F the Faraday constant. Thus, integration of Eq. 6 with the proper initial conditions yields to $\theta(t)$ and hence to $I(t)$ from Eq. 7.

2.3. Classical derivation of steady state behaviour and ac impedance response

In traditional electrochemistry, the complex impedance is measured and modelled at the steady-state defined by $\frac{d\theta}{dt} = 0$ in Eq.6. Assuming that θ_s is the steady-state value of θ at an imposed potential E_s , Eqs. 6 and 7 lead to the following expression of the steady-state current density:

$$j = F z_d K_d \frac{1}{\left(\frac{K_d}{K'_p} + 1 \right)} \quad (8)$$

It is noteworthy that j depends only on θ_s , *i.e.* on the ratio $\frac{K_d}{K'_p}$ and not on the absolute values of these constants. Only a time or frequency resolved measurement is able to evaluate these quantities in the model.

Eqs. 6 and 7, take respectively their differential forms as Eqs. 9 and 10 for a sine wave modulation $\Delta E = |\Delta E| \exp(j\omega t)$ of the applied potential around the steady-state value E_s where $|\Delta E|$ is small enough for neglecting the contribution of higher orders terms (linear approximation) and the constants K_p and K'_p have their values for E_s .

$$\beta j \omega \Delta \theta = \left(\frac{\Delta K_p}{\Delta E} (1 - \theta_s) - \frac{\Delta K'_p}{\Delta E} \theta_s \right) \Delta E - (K_p + K'_p) \Delta \theta \quad (9)$$

$$\Delta j = F \left[z_p \left(\frac{\Delta K_p}{\Delta E} (1 - \theta_s) - \frac{\Delta K'_p}{\Delta E} \theta_s - \frac{\Delta \theta}{\Delta E} (\Delta K_p + \Delta K'_p) \right) + z_d \left(\frac{\Delta K_d}{\Delta E} (1 - \theta_s) - \frac{\Delta \theta}{\Delta E} \Delta K_p \right) \right] \Delta E \quad (10)$$

The reaction steps are assumed to obey Tafel laws, expressed in their simplified form:

$K_p = k_p \exp(b_p E)$, $K'_p = k'_p \exp(b'_p E)$, $K_d = k_d \exp(b_d E)$ in which b_p and $b_d > 0$ and $b'_p < 0$ are in V^{-1} .

Finally by extracting from Eq. 9 the expression of $\frac{\Delta \theta}{\Delta E}$:

$$\frac{\Delta \theta}{\Delta E} = \frac{K_p b_p (1 - \theta_s) - K'_p b'_p \theta_s}{\beta j \omega + K_p + K'_p} \quad (11)$$

The admittance on a surface unit, Z^{-1} can be expressed as:

$$\frac{\Delta j}{\Delta E} = \frac{\Delta j_d}{\Delta E} + \frac{\Delta j_p}{\Delta E} = F \left[z_d K_d \left(b_d (1 - \theta_s) - \frac{\Delta \theta}{\Delta E} \right) + z_p \beta j \omega \frac{\Delta \theta}{\Delta E} \right] \quad (12)$$

where one can see that the frequency dependence of Z arises only from the frequency response of the coverage θ given by Eq. 11.

2.4. Derivation of the dc and ac responses associated to the travelling transient

The transient behaviour sketched in Fig. 1 can now be deduced from the model. The pin position is taken as the origin of the time σ and distance x scales. The derivation is done according to the following steps:

- Determination of $\theta(\sigma)$ by integration of Eq. 6 with $\theta(0) = 0$ (corresponding to a bare surface condition) when the pin position is at $\sigma = 0$;
- Derivation of the transient $j(\sigma)$ by introducing $\theta(\sigma)$ in Eq. 7;
- Derivation of the admittance density at position σ by introducing the local value $\theta(\sigma)$ in Eq. 10 and the local value of $\frac{\Delta \theta}{\Delta E}(\sigma)$ in Eq. 12.

Finally, the ac response of the whole abraded track is calculated from Eq. 5.

3. Experimental

3.1. Mechanical device

A rotating pin in a Pin-on-Disc tribometer, (Multi-Spécimen Falex - Compass Instrument) was used. The abrading surface made of polished fritted zircon has a curvature radius of 100 mm. The load was controlled by the tribometer to 5 Newton for all the data dealt with in this paper.

At the end of a set of electrochemical measurements, the tacks were analysed by optical profilometry with a chromatic confocal point sensor CHR 150-N (Stil, Aix en Provence,

France)

3.2. Electrochemical conditions

The disc electrode consisted of a 304L stainless steel bar of 0.9 cm in diameter laterally insulated by an epoxy resin. The electrolyte was 0.5 M H₂SO₄ solution and the potential was measured with respect to an Ag/AgCl reference electrode. Three values of the rotation speed were used, 20, 40, and 60 rotations per minute (RPM). The size of the abraded track was 0.45 cm in diameter. The non-abraded area was fully exposed to the electrolytic solution; therefore its own contribution was measured separately and subtracted from the global data in order to extract the specific response of the abraded area. Preliminary experiments were performed at two electrode potentials, 0 and 0.3 V/Ag/AgCl. Most of the results presented in this paper are relative to 0 V/Ag/AgCl.

4. Results and discussion

4.1. Steady-state current-voltage curve of the non-abraded stainless steel

The quasi-steady state (1 mVs⁻¹) current-voltage curve of the SS is shown in Fig. 4. It displays the typical profile of this material: successively an activity peak, an active-passive transition with a negative slope, a passivity plateau and a transpassive dissolution range. The domain of interest for the tribocorrosion behaviour is the passivity range where the material is protected by a very thin film and its corrosion possibly affected by abrasion. The latter may results in a polarisation of a small part of the electrode at a potential in the passivity domain without the protection of the passive film.

Fig. 5 shows the current dependency as a function of the rotation rate of the P-o-D and for two different potentials. Interestingly, both curves shows the same trend (a linear variation in a semi-logarithmic scale) and a slope of $2.1 \cdot 10^{-5} \text{ A cm}^{-1}\text{s}$ was determined. After the experiment,

the surface area of the track was 0.077 cm^2 . However, in this particular case, normalized values with respect to the surface area make no sense since these are only averages over the entire transient and no direct comparison can be done between the current and the impedance.

Additionally, numerical simulations of the current from Eq. 4 (red curve of Fig. 6) allowed the evaluation of the ratio $\frac{T}{\tau}$ and then the lower limit for which the system behaves linearly.

Fig. 7 shows the cross section of the abraded track measured by optical observations at the end of a set of experiment. These observations allowed to evaluate the area of the abraded surface and to verify that the curvature corresponds to that of the pin used in the experiment.

Taking into account the width w (0.055 cm) of the track, assimilated to a flat surface in Fig.7, the slope deduced from Fig. 5, $2.1 \cdot 10^{-5} \text{ A cm}^{-1}\text{s}$, is converted into the mean charge density involved in the transient: $2.1 \cdot 10^{-5} / 0.055 = 381 \text{ } \mu\text{C cm}^{-2}$. For an exponential form of the current density with a time-constant τ , this charge corresponds to an initial peak $j_0 = 381 \text{ } \mu\text{C.cm}^{-2}/\tau$. For every rotation rate, a boundary is plotted on Fig. 4 indicating the lower limit of j_0 allowing to match the condition $T / \tau > 2.13$ defined on Fig. 6. As shown in Fig. 4, at the working potential $E = 0 \text{ V/Ag/AgCl}$, a likely current density on a bare surface as it is extrapolated from a Tafel line in the activity range, does fall well below these limits for the 3 rotation rates. However this comparison in terms of steady-state does not account for the charges consumed in the film growth which flow only in transient regime. This is why the foregoing part of this paper is devoted to EIS measurement and interpretation under abrasion aimed at separating the two components of the transient current. The model presented in Fig. 3 has been used for computing in a first step the steady-state current density-potential plot. The set of parameters is presented in Table1.

The data yielded by the model were $\tau = 0.197$ s and a current density of $0.154 \text{ mA}\cdot\text{cm}^{-2}$ for a bare surface at $E = 0 \text{ V/Ag/AgCl}$. This current density is clearly smaller than the minimal value associated to $\tau = 0.197$ s determined with the relation $j_0 = 381 \mu\text{C cm}^{-2}/\tau$, namely $j_0 = 1.93 \text{ mA}\cdot\text{cm}^{-2}$, and therefore well below the lower limits of j_0 for the 3 rotation speeds as shown in Fig. 5. However, it must be considered that, as shown in Fig.1, the whole transient and its initial value at $\sigma = 0$, are associated not only to the dissolution rate but also to the film recovery. Therefore the model can only be evaluated by considering the whole electrochemical response including the ac impedance. The impedance has been measured at 0 V/Ag/AgCl over the frequency range $62 \text{ kHz} - 0.016 \text{ Hz}$ with 7 frequencies per decade and an *ac* amplitude of $30 \text{ mV}_{\text{rms}}$. The raw data have been corrected of the contribution from the large non-abraded passive area surrounding the track. Fig. 9 shows the experimental Nyquist plot of the measured impedance and the impedance of the track alone.

The track impedance shows a short HF inflexion in the positive real quadrant, bends to the left and then intersects the imaginary axis clearly tending to a negative real limit at lower frequencies. This behaviour in classical steady-state conditions is associated to a negative-sloped current-voltage curve, *i.e.* to passivation [18,17,16]. This is intuitively consistent with the film regrowth process that takes place behind the pin. However a more rigorous validation of the model is provided only by comparing the impedance diagrams at the three different rotation rates investigated to the simulated ones. In order to apply Eq. 5, the local admittances, $a(E_0, \sigma, j\omega)$ was computed along the transient at a series of σ values between 0 and 3τ . Then the averaged value of the impedance was rescaled taking into account the track width w and the velocity v following Eq. 5. Fig. 10 shows some of the impedance plots calculated at several σ/τ values and the corresponding points on the $j(\sigma)$ curve in the insert. The averaged Z plot holds for the simulated response of the whole track. As expected, at short times a

higher current density is associated to a lower impedance. The diagrams display a shape quite similar to the experimental one shown in Fig. 9 with a negative low frequency limit on the real axis. Averaged computed impedances for the three rpm, once rescaled can be compared to the experimental diagrams presented in Fig. 11. A fairly good agreement is found in terms of size, shape and frequency. The impedance is exactly inversely proportional to the abrasion velocity since, as highlighted by the model, the same $j(\sigma)$ transient is spread to an area proportional to the velocity.

It should be stated that, in order to approach a correct simulation in the high frequency range, essentially determined by the capacitive, dielectric-like response, not taken into account in the reactive model, an unusually large double-layer capacitance had to be used, namely of the order of 1 mF cm^{-2} . That happened essentially for small σ values (that is for the beginning of the transient response) where the double layer is only starting to build-up. As far as we know, there are no available data on the capacitance value under these conditions, which are not accessible in classical experiments. However it can be reasonably inferred that the double layer is thinner than at its equilibrium and therefore exhibits a larger capacitance.

4.2. Interpretation in terms of contributions to the total wear

The model can be regarded as accounting correctly for both the steady-state and the transient responses of the interface under abrasion in corrosive conditions. It yields a new way of collecting quantitative information on the relative contributions of the film repair and active dissolution taking place on the freshly bared surface.

As shown in Fig. 12 both components are very close to an exponential decay in agreement with the first order differential equation Eq. 6. The ratio $\frac{i_p}{i_d}$ is about 12 over the whole time range. It is clear that even in this aggressive media, the major part of the current under

abrasion is due to the film repair, not to the direct active dissolution of the unprotected surface. It can be considered that the reactive part of the total wear is traduced in i_p . This ratio of 12 may be regarded as a minimum since the β value in Table 1 is equivalent to a passive film of one to two monolayers thick, only. A larger β would of course led to an even larger ratio. The total wear measured on the track profile shown in Fig. 7 is *a priori* due to the sum of the reactive contribution, essentially i_p , and a likely pure mechanical wear of the underlying metal as represented in Fig. 1. This pure mechanical wear can be estimated by comparing the damaged profile to the faradic equivalent of $i_p + i_d$. A rough estimation by ascribing a dissolution valency of 2 to the removed material yields a charge of about 1 C. This charge, taking into account the charge density flowing under the transient ($381 \mu\text{C}\cdot\text{cm}^{-2}$), the track area (0.077 cm^2) would require about 34000 rotations. This figure is far larger than the cumulated number of rotations during the whole series of measurements, estimated to 10000. It can thus be concluded that the pure mechanical damage can be estimated to 71 % of the total wear.

5. Conclusions

The use of a pin-on-disc tribometer allows a pseudo-steady-state to be reached and thus electrochemical impedance measurements to be performed. A general approach is proposed for interpreting the ac response of the current due to abrasion in an electrochemical environment in the framework of the accepted model in triboelectrochemistry. Application to a stainless steel submitted to a permanent friction by a pin-on-disc tribometer in acidic medium established that a traditional electrochemical model of dissolution-repassivation can interpret at the same time the electrochemical behaviour (current-voltage curve and impedance spectra), as well as the response of the non-abraded material for three different rates of abrasion. The main advances lie in the possibility of extracting separately the contribution of the film recovery and that of the direct dissolution to the overall current, which finally lead to better understanding the wear mechanism. More generally, the use of

traditional techniques in tribocorrosion tests, like polarisation resistance, is likely to be more rigorously assessed.

List of symbols

$a(E_0, \sigma, j\omega)$	local admittance density
b_i	Tafel coefficient of the reaction i
E	electrochemical potential
$ \Delta E $	amplitude of the sine wave perturbation for an EIS experiment
F	Faraday constant
\vec{F}_n	load applied by the tribometer
\vec{F}_t	friction force
$I(L)$	local current density along the wear
$j(\sigma)$	current density
j_0	current density at $\sigma = 0$
j_d	current density ascribed to the anodic dissolution of bare metal
j_p	current density of the passive film regrowth
K_i	kinetic constant of the reaction i
L	length of the abraded area
S	surface area
T	the time-window considered in the experiment
v	velocity of the abrading body
w	width of the abraded area
z_i	number of electron exchanged in the reaction i
Z	electrochemical impedance

- β surface concentration of the film
- θ surface fraction coverage
- θ_s surface fraction coverage at steady-state
- σ time variable referring to the position of the sliding abrasive body (at $\sigma = 0$)
- τ time constant of the exponential current decay
- ω angular frequency ($\omega = 2\pi f$)

References

1. Landolt D, Mischler S, Stemp M (2001) Electrochemical methods in tribocorrosion: a critical appraisal. *Electrochim Acta* 46:3913-3929
2. Takadoum J (1996) The influence of potential on the tribocorrosion of nickel and iron in sulfuric acid solution. *Corros Sci* 38:643-654
3. Favero M, Stadelmann P, Mischler S (2006) Effect of the applied potential of the near surface microstructure of a 316L steel submitted to tribocorrosion in sulfuric acid. *Journal of Physics D: Applied Physics* 39:3175-3183
4. Keddam M, Wenger F (2011) Electrochemical methods in tribocorrosion. In: *Tribocorrosion of Passive Metals and Coatings*. pp 187-221
5. Ponthiaux P, Wenger F, Drees D, Celis JP (2004) Electrochemical techniques for studying tribocorrosion processes. *Wear* 256:459-468
6. Guadalupe Maldonado S, Mischler S, Cantoni M, Chitty WJ, Falcand C, Hertz D (2013) Mechanical and chemical mechanisms in the tribocorrosion of a Stellite type alloy. *Wear* 308:213-221
7. Déforge D, Huet F, Nogueira RP, Ponthiaux P, Wenger F (2006) Electrochemical noise analysis of tribocorrosion processes under steady-state friction regime. *Corrosion* 62:514-521
8. Keddam M, Ponthiaux P, Vivier V (2014) Tribo-electrochemical impedance: A new technique for mechanistic study in tribocorrosion. *Electrochim Acta* 124:3-8.
9. Azzi M, Klemberg-Sapieha JE (2011) Tribocorrosion test protocols for sliding contacts. In: *Tribocorrosion of Passive Metals and Coatings*. pp 222-238
10. García I, Drees D, Celis JP (2001) Corrosion-wear of passivating materials in sliding contacts based on a concept of active wear track area. *Wear* 249:452-460
11. Isaacs HS, Ryan MP, Oblonsky LJ (1997) Mapping currents at the corroding surface/solution interface. *ProcCorros/97 ResTopSymp*:65-79

12. Tallman DE, He J, Gelling VJ, Bierwagen GP, Wallace GG (2003) Scanning vibrating electrode studies of electroactive conducting polymers on active metals. ACS SympSer 843 (Electroactive Polymers for Corrosion Control):228-253
13. Bayet E, Huet F, Keddam M, Ogle K, Takenouti H (1999) Local electrochemical impedance measurement: scanning vibrating electrode technique in ac mode. Electrochim Acta 44 (24):4117-4127
14. Annergren I, Thierry D, Zou F (1997) Localized electrochemical impedance spectroscopy for studying pitting corrosion on stainless steels. J Electrochem Soc 144:1208-1215
15. Huang VM-W, Wu S-L, Orazem ME, Pebere N, Tribollet B, Vivier V (2011) Local electrochemical impedance spectroscopy: A review and some recent developments. Electrochim Acta 56:8048-8057
16. Keddam M (2006) 2006 W.R. Whitney Award Lecture: application of advanced electrochemical techniques and concepts to corrosion phenomena. Corrosion 62:1056-1066.
17. Keddam M, Mattos OR, Takenouti H (1981) Reaction model for iron dissolution studied by electrode impedance. II. Determination of the reaction model. J Electrochem Soc 128:266-274
18. Keddam M, Mattos OR, Takenouti H (1986) Mechanism of anodic dissolution of iron-chromium alloys investigated by electrode impedances - II. Elaboration of the reaction model. Electrochim Acta 31:1159-1165

Captions

Table 1: parameters values used for simulating the dc and ac behaviours of the model in Fig.3

Fig. 1: Model of the mechanical effect of a rubbing contact on a passive material and of its subsequent electrochemical responses. The protecting film, (in green), is totally removed and the pin ploughs somehow in the underlying metal, (in blue). Behind the pin, two parallel processes take place: healing of the damage by film regrowth and dissolution of the incompletely protected metal. Each of them gives rise to a separate component, j_p and j_d of the total current density $j(E, x(\sigma))$. \vec{F}_n is the load, \vec{F}_t the friction force, v the velocity, and E the applied electrochemical potential.

Fig. 2: Effect of a small amplitude ac modulation of the applied potential at E_0 . The transient current oscillates between the two bounds in dashed line. The local current density, Δj , at the time σ or distance $v\sigma$ of the pin is determined by the local admittance density: $a(E_0, \sigma, j\omega)$.

Fig. 3: Sketch of the components depicting a reversible passivation-depassivation and dissolution of the bare area. The rate constant K 's are supposed to depend on the applied potential E on Fig. 1. At any instant and for a given E value, the state of the interface is totally determined by the value of the surface fraction θ occupied by the film.

Fig. 4: Quasi-steady state (1 mVs^{-1}) current-voltage curve of the 304L SS in $0.5\text{M H}_2\text{SO}_4$ solution. The horizontal dashed lines indicate the lower limits of the current density $j_0 = j(0)$ compatible with the results shown in Fig. 5. The red dot at 0.154 mA cm^{-2} corresponds to the dc current density predicted by the model presented Fig. 3 for a totally bare surface at $E = 0 \text{ V/Ag/AgCl}$.

Fig. 5: Dependence of the current under abrasion at two potentials (0 and 0.3 V/Ag/AgCl) on the rotation speed in RPM (lower scale) and the linear velocity, v , (upper scale). Dashed line is a least squares fit on both RPM set of data. The slope $2.1 \cdot 10^{-5} \text{ A cm}^{-1}\text{s}$ is the mean charge flowing through electrochemical reactions along 1 cm length of the actual track of width w . The surface area of the track was 0.077 cm^2 .

Fig. 6: Simulation of the $I(v)$ dependence following Eq. 4 for $j_0 = 1 \text{ mAcm}^{-2}$, $w = 1 \text{ mm}$, $L = 1.42 \text{ cm}$ (actual length of the track). As predicted by Eq. 4, $I \cong v j_0 \tau$ for values of $T \geq \tau$ where the transient is totally contained in the rotation period. It tends towards the limit $j_0 L$ for $T \gg \tau$, i.e. when the current transient remains close to its initial value at $t=0$ over the whole rotation period. A value of about 2 for the T / τ ratio, (orange dashed line) can be accepted as a lower limit for observing a nearly linear dependence (green dashed line).

Fig. 7: Radial cross-section of the abraded track at the end of the whole series of experiments. Area of the wear section: $2800 \mu\text{m}^2$. The curvature is that of the pin apex.

Fig. 8: Steady-state profiles of the current density-potential and surface coverage θ by the passive film computed with the model. The set of parameters, given in Table 1, was optimised by trial-and-error accounting for both the steady-state and the ac impedance. Note that the tangent to the curves plotted with the Tafel slope of the anodic dissolution reaction (see Table 1) is close to the experimental one. It is extrapolated to obtain the dissolution rate of bare surface at $E = 0 \text{ V/Ag/AgCl}$. The passive current plateau and the cathodic component were rendered by introducing respectively a low solubility of the film (rate $2 \cdot 10^{-12} \theta$) and a proton reduction (rate $2 \cdot 10^{-14} \exp(-19.E)$). They have no influence on the behaviour investigated in this paper.

Fig. 9: Nyquist plots of the raw data (red triangles), and of the impedance of the abraded track alone (blue circles), after correcting for the contribution of the passive area in $0.5 \text{ M H}_2\text{SO}_4$ at $E = 0 \text{ V/Ag/AgCl}$. $|\vec{F}_n| = 5 \text{ Newtons}$, 40 rpm .

Fig. 10: Simulated local impedance densities at various σ values marked on the $j(\sigma)$ profile (insert) and impedance density averaged over the whole transient for 60 rpm .

Fig. 11: Comparison of the experimental (a) and simulated (b) Nyquist plots of the whole track impedance at 3 rotation speeds in the experimental range of frequency.

Fig.12: dissolution i_a and passivation i_p components of the overall transient current as a function of the reduced time σ / τ .

Table and figures

Table 1

$k_d, \text{Mole.s}^{-1} \text{cm}^{-2}$	$k_p, \text{Mole.s}^{-1} \text{cm}^{-2}$	$k'_p, \text{Mole.s}^{-1} \text{cm}^{-2}$	b_d, V^{-1}	b_p, V^{-1}	b'_p, V^{-1}	$\beta_i, \text{Mole.cm}^{-2}$	Z_d	Z_p
$8 \cdot 10^{-10}$	$6.6 \cdot 10^{-9}$	$5.4 \cdot 10^{-12}$	6	21	-21	$1.3 \cdot 10^{-9}$	2	3

Figure 1

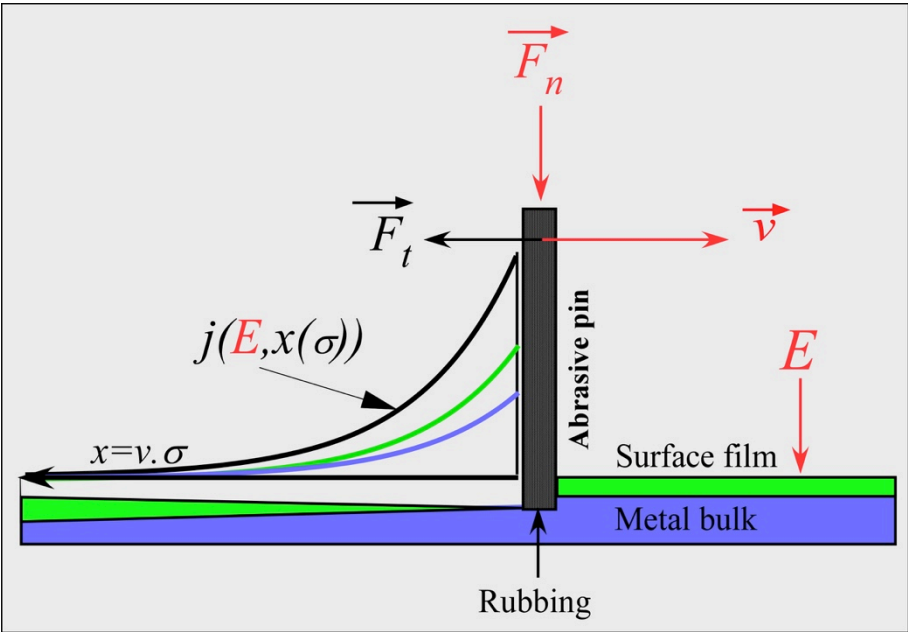


Figure 2

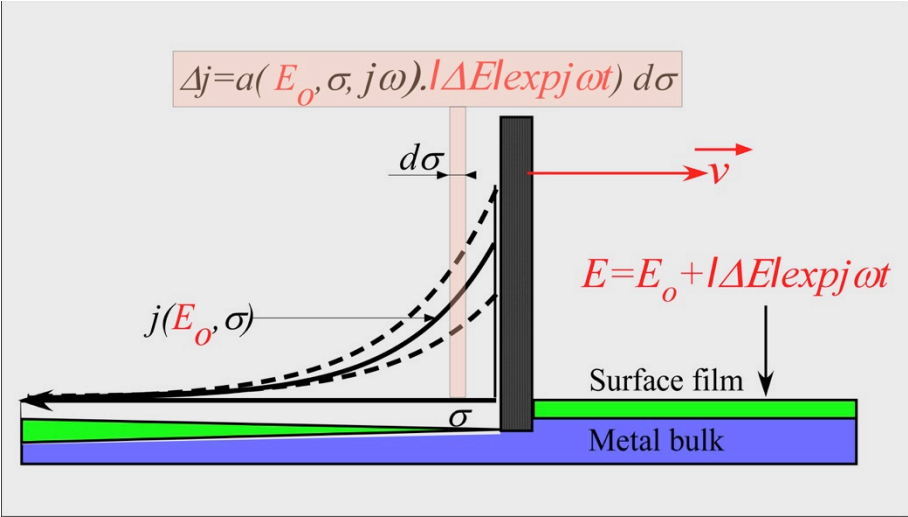


Figure 3

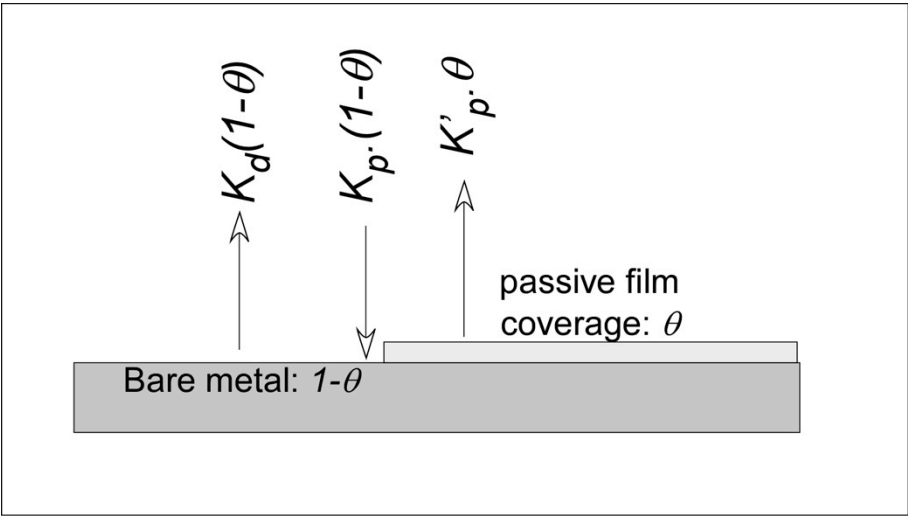


Figure 4

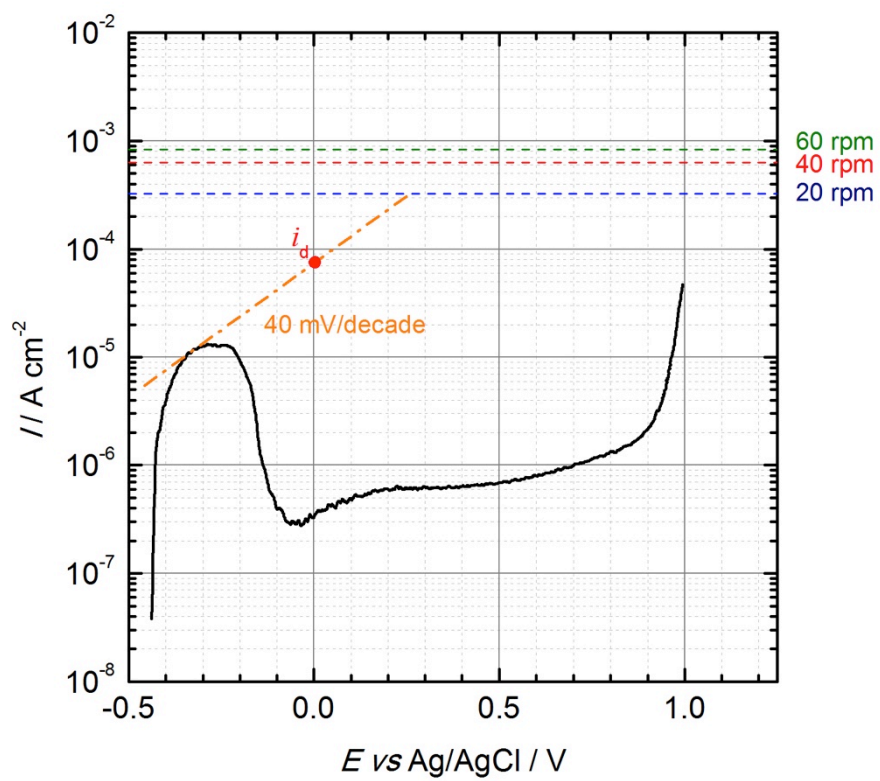


Figure 5

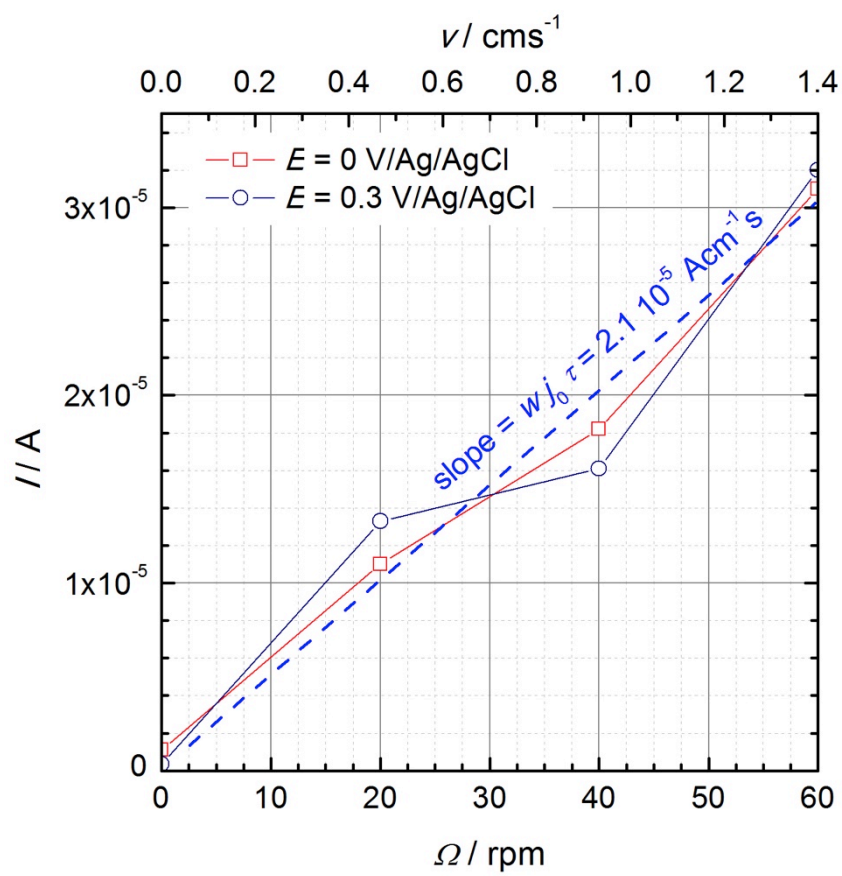


Figure 6

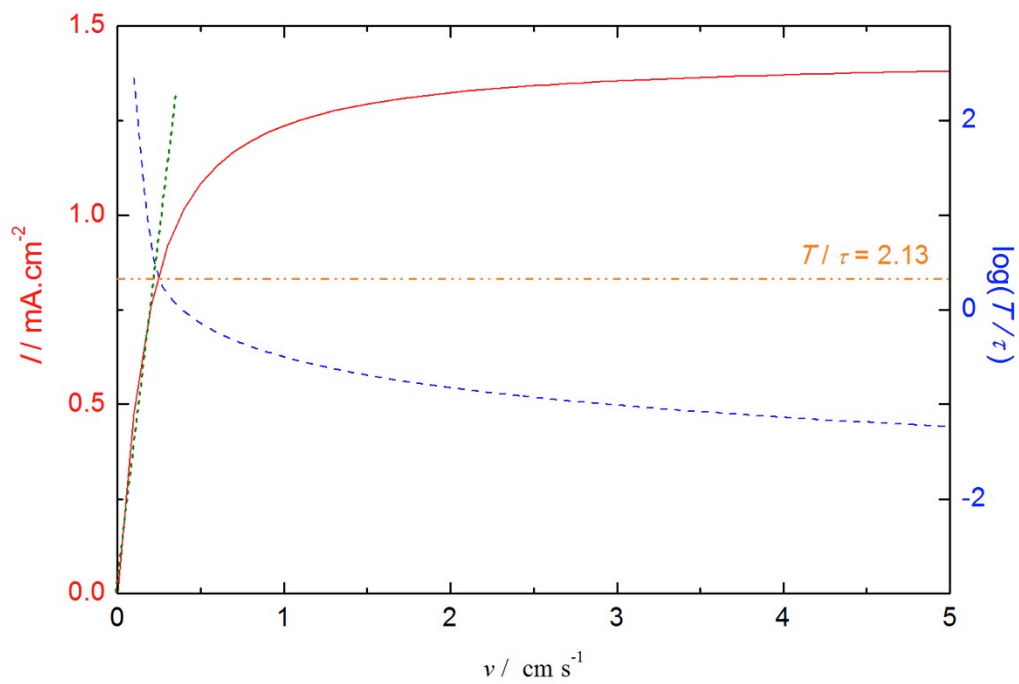


Figure 7

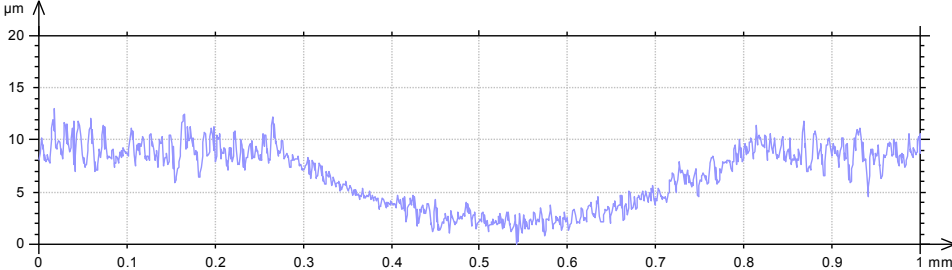


Figure 8

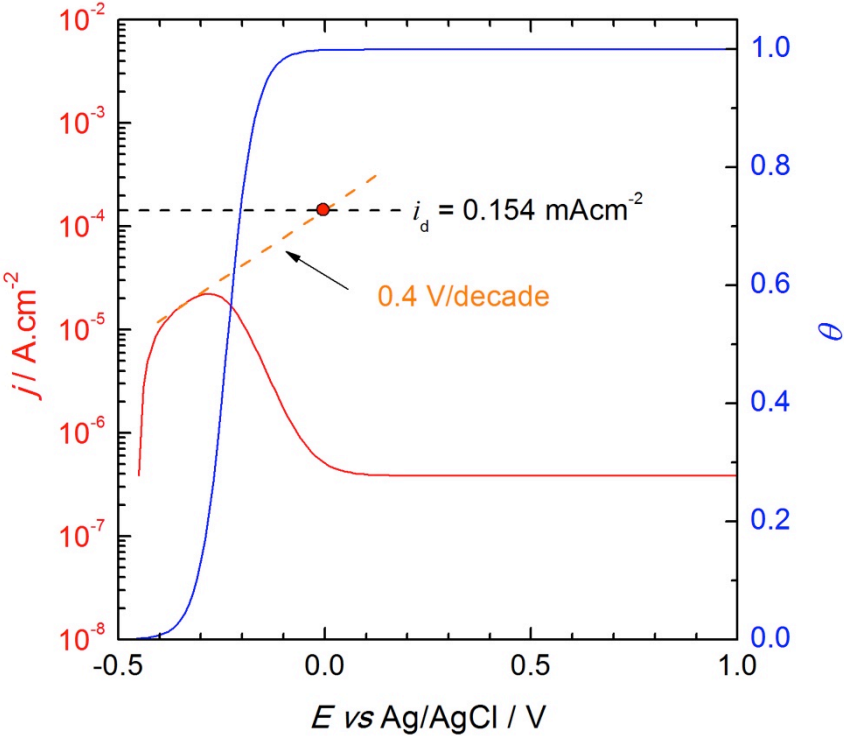


Figure 9

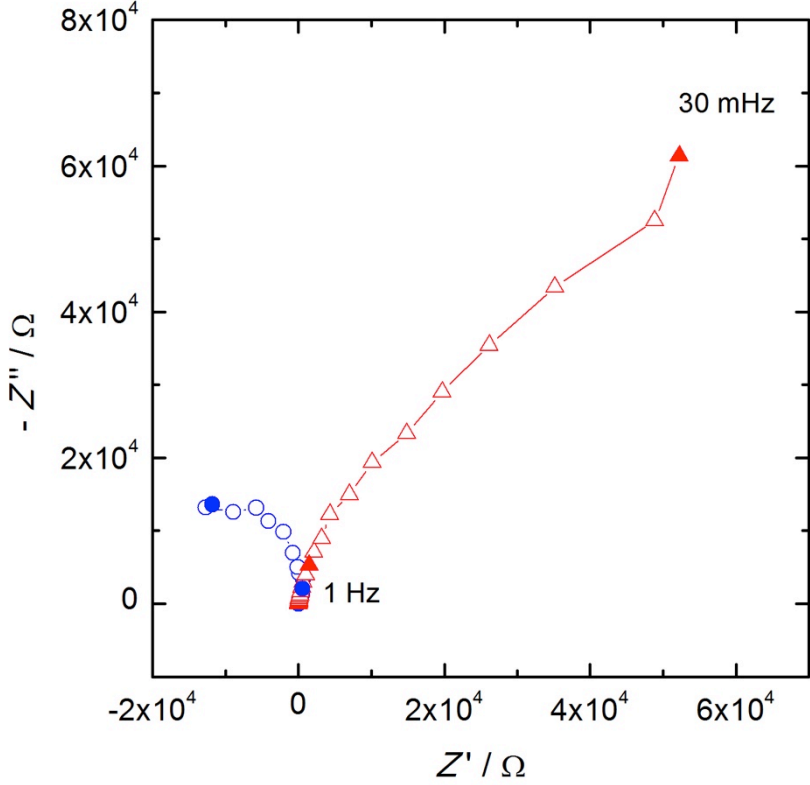


Figure 10

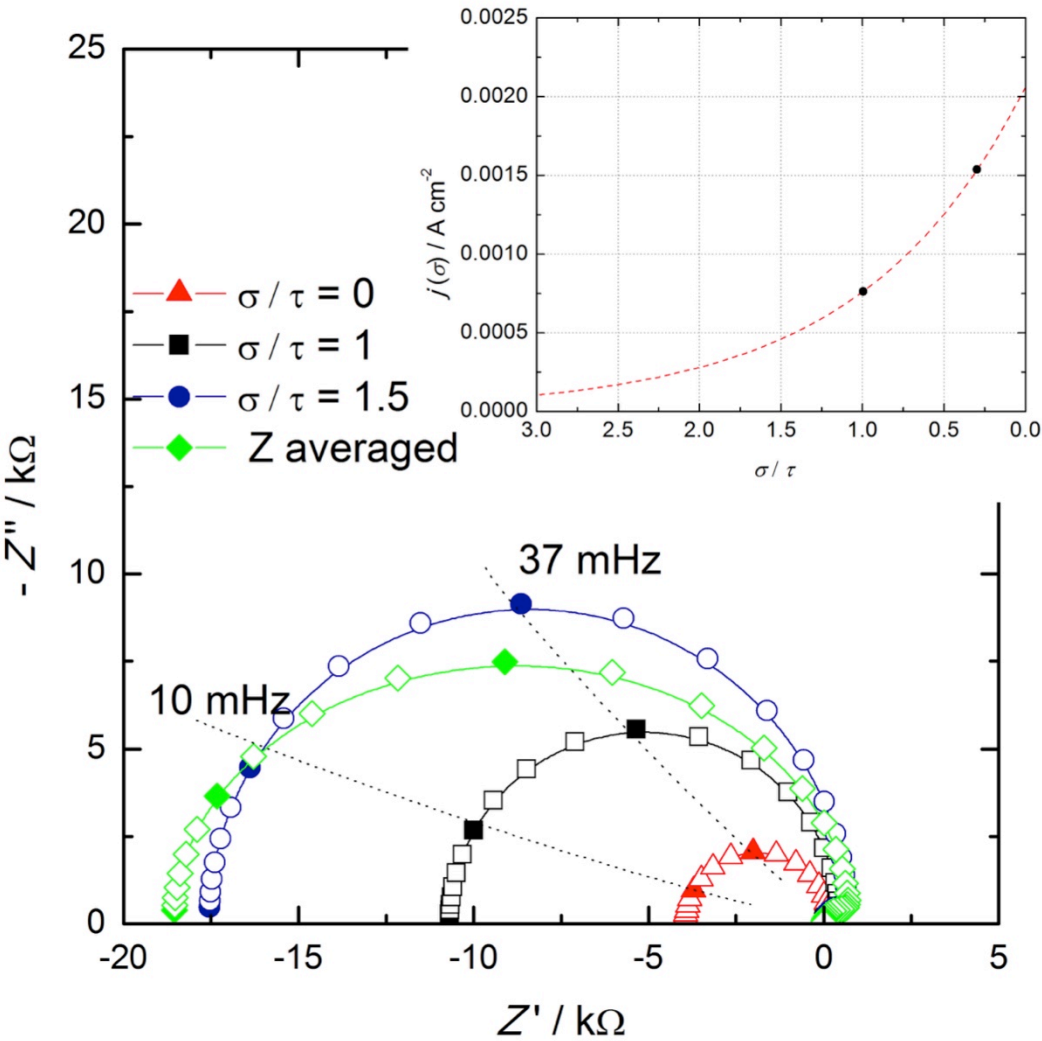


Figure 11

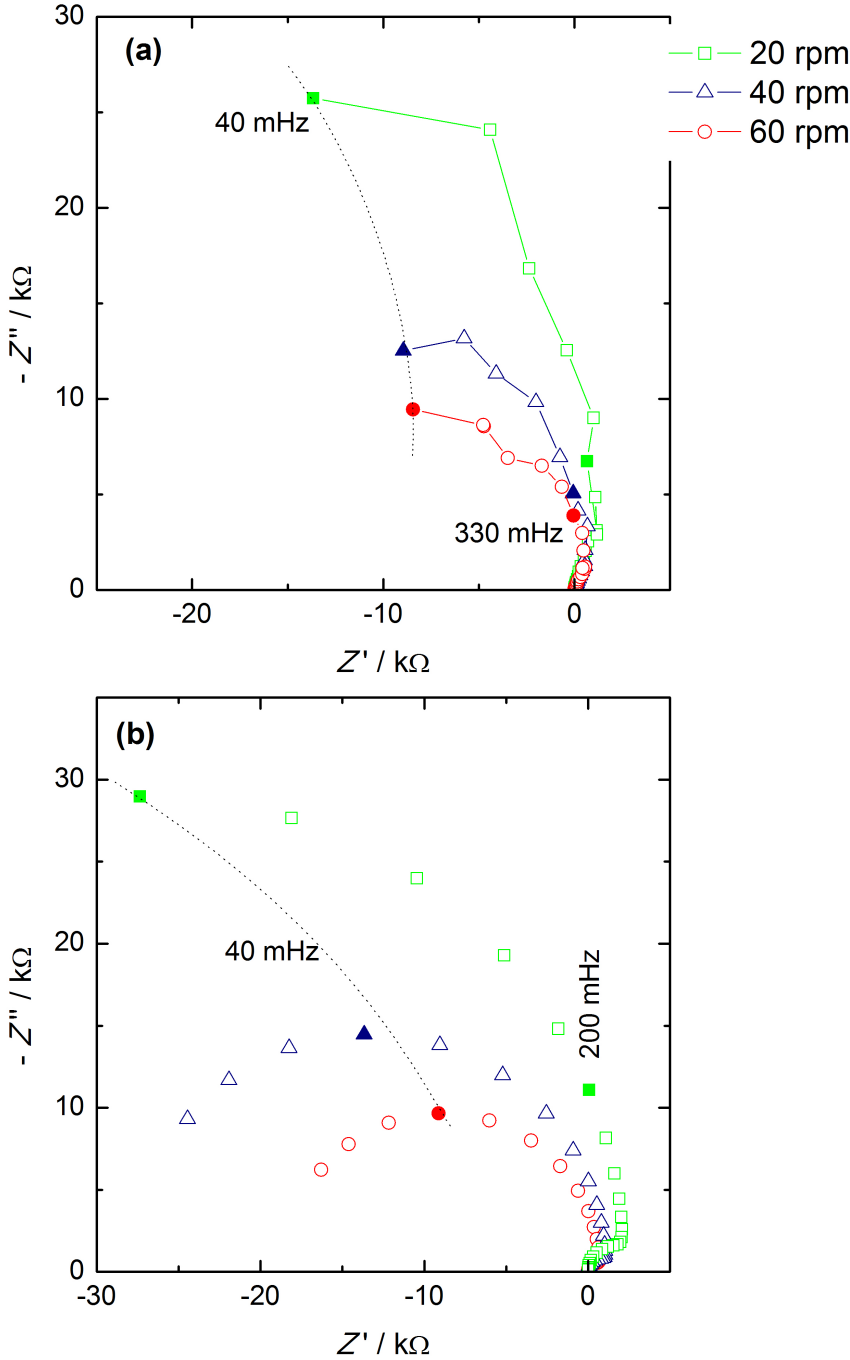


Figure 12

